Organic & Biomolecular Chemistry

ROYAL SOCIETY OF CHEMISTRY

PAPER

View Article Online
View Journal | View Issue

Cite this: *Org. Biomol. Chem.*, 2025, **23**, 8704

Interaction studies by NMR on the multivalent interaction between chondroitin sulfate E derivatives and the langerin receptor

M. José García-Jiménez,†[a] Sergi Gil,†[a] Pedro Domínguez-Rodriguez,[a] Laura Roldán,[a] Michel Thepaut,[b] Francisco Arrabal-Campos,[c] Ignacio Fernandez,[c,d] Franck Fieschi,[b,e] Javier Rojo,[a] José. L. de Paz[a] and Pedro M. Nieto*[a]

In this paper, we present the NMR analysis of multivalent compounds displaying chondroitin sulfate E (CS-E) disaccharide ligands and their interaction with langerin. The disaccharides correspond to the two alternative sequences of CS-E: GlcA–GalNAc and GalNAc–GlcA. Firstly, we studied the conformation of the two corresponding series of glycodendrimers free in solution and in the presence of langerin. The NMR structures of the free compounds are compatible with the expected ones. Both sequences exhibit very similar conformations with a rigid moiety, the disaccharides, and a flexible region corresponding to the rest of the molecule. A key aspect of this work is the detailed analysis of how different compounds interact with distinct regions of the langerin receptor as a function of the spatial distribution of the same binding epitope. This allows us to gain unique insights into the receptor's binding behavior and the specific interactions mediated by different ligand multivalency. We conducted transferred NOESY experiments in the presence of langerin, concluding that the conformations of the bound disaccharides were the same as the free ones. In addition, we performed STD-NMR experiments and analyzed the binding epitope, demonstrating that the monovalent compound with GlcA at the non-reducing end can interact with langerin through the Ca^{2+} cation, while the reverse sequence does not. The corresponding trimers **2** and **6** interact mainly *via* the central aromatic core, independent of the disaccharide sequence. In the case of tetramer **3**, the interaction takes place mainly by the GalNAc proton in position 4 and in the hexamer, significant spin diffusion prevents epitope analysis, although the interaction with langerin is clearly observed. The STD-NMR experiments in the absence of Ca^{2+} showed a lack of binding for both monovalent compounds **1** and **5**. In contrast, in the case of multivalent compounds **2**, **3** and **6**, STD peak characteristics of binding were found with similar pattern epitope maps to those obtained in the presence of Ca^{2+}. We also performed DOSY experiments for the first series of GlcA–GalNAc compounds individually, in the presence and absence of langerin, and for the mixture of all the compounds in the same NMR tube. Finally, we performed MD simulations for the monovalent and trivalent compounds, corroborating the NMR analysis for the compounds in the absence of langerin.

Received 20th May 2025,
Accepted 21st August 2025

DOI: 10.1039/d5ob00845j

rsc.li/obc

Introduction

Glycosaminoglycans (GAGs) are a class of extracellular polysaccharides commonly found conjugated with proteins that play pivotal roles in many biological functions from embryonic development to the regulation of signaling within the extracellular matrix (ECM).[1] Chondroitin sulfate (CS) belongs to the glycosaminoglycan family and comprises alternating units of *N*-acetyl-D-galactosamine and D-glucuronic acid linked by β-1–3 and β-1–4 glycosidic bonds. CS is involved in critical biochemical processes such as angiogenesis, cancer, inflammation, and host–pathogen interactions, primarily through their inter-

[a]*Glycosystems Laboratory, Instituto de Investigaciones Químicas (IIQ), Centro de Investigaciones Científicas Isla de La Cartuja, CSIC and Universidad de Sevilla, 41092 Sevilla, Spain. E-mail: pedro.nieto@csic.es*
[b]*Université Grenoble Alpes, CNRS, CEA, IBS, F-38044 Grenoble, France*
[c]*Department of Chemistry and Physics, ceiA3, Universidad de Almería, Almería, Spain*
[d]*BITAL, Research Centre for Agricultural and Food Biotechnology, Almería, Spain*
[e]*Institut Universitaire de France (IUF), France*
†These authors contributed equally.

actions with other signaling proteins.[2,3] The structural heterogeneity of CS lies in the uneven distribution of *O*-sulfated groups along its chains. However, the precise "sulfation code" that governs its biological activity remains elusive.[2]

Two binding sites have been described for GAG and langerin: the lectin C site[4] and a long cleft between two of the three CRDs (Carbohydrate Recognition Domains) and the helices of the trimeric neck.[5] The lectin site accommodates GAG fragments in a Ca^{2+} dependent mode when the non-reducing end carries two contiguous hydroxyl groups in a *trans*-diequatorial disposition. The other binding site corresponding to longer saccharidic sequences is independent of Ca^{2+} and it is in the interphase between two of the three domains of langerin.

In our previous work,[6–9] we synthesized oligosaccharides that represent chondroitin sulfate, particularly type E, and examined their interactions with midkine and pleiotrophin.[6–9] We also synthesized and characterized first- and second-generation dendrimers as glycomimetics of CS structures and investigated their binding properties with langerin, a C-type lectin receptor implicated in immune response regulation.[10,11] Building upon these findings, this study investigates into the structural properties of selected first-generation dendrimers by comparing their interactions with langerin as a function of the degree of valence and also considering equivalent dendrimers with reverse sequences with larger resolution methods.[10,11]

Central to our investigation is the exploration of langerin interaction mechanisms in the presence and absence of Ca^{2+} ions,[4,12] assuming the recognition mediated by a Ca^{2+} ion in the carbohydrate recognition domain (CRD) as the primary binding site. Additionally, we aim to elucidate potential sequence-dependent binding selectivity, probing the possibility of altering binding sites to modulate the lectin activity.

To gain further insights into ligand–receptor interactions, we employ NMR analysis utilizing ligand-observed or transient methods.[2] This provides valuable structural information essential for understanding the intricate interplay between CS mimetics and langerin. The idea that varying the binding site of the lectin can modify its activity is attractive.[10,13]

Results and discussion

Synthetic procedures

In this study, we have considered the compounds shown in Fig. 1. The preparation of the derivatives presenting the GlcA–GalNAc disaccharide (**1–4**) has been previously reported.[10] For the synthesis of multivalent systems displaying the GalNAc–GlcA sequence, we first prepared disaccharide ligand **8** (Scheme 1). For this purpose, we required a GlcA building block containing an orthogonal protecting group at position 4, trichloroacetimidate **9**.[14–16] Glycosylation between **9** and 3-bromo-1-propanol afforded the desired β-glycoside **10**. Selective deprotection of the levulinoyl (Lev) group was accomplished with hydrazine monohydrate to give glycosyl acceptor **11** in excellent yield. Monosaccharide **11** was then glycosylated with galactosamine donor **12**,[17] using TMSOTf as a promoter, to give disaccharide **13** in good yield. Substitution of the bromide by an azido group was performed by treatment with sodium azide at room temperature in DMF to obtain compound **14**. The azido moiety was key for further conjugation of the disaccharide ligand with the dendritic cores. Next, acetyl groups were selectively removed by treatment with *p*-toluenesulfonic acid (*p*-TsOH) in CH_2Cl_2/MeOH to afford disaccharide **15**. Treatment with di-*tert*-butylsilyl bis(trifluoromethanesulfonate) $tBu_2Si(OTf)_2$ in pyridine gave compound **16** with a cyclic silylene group protecting the OH-4 and OH-6 of the GalNAc unit. Acetylation at position 3 yielded disaccharide **17**. The cyclic silylene group was then selectively removed using the $(HF)_n$·Py complex in THF and the released hydroxyls were subsequently sulfated with SO_3·Me_3N in DMF under microwave (MW) irradiation to obtain compound **18**. Finally, basic hydrolysis of ester and amide groups using NaOH followed by selective *N*-acetylation gave the disulfated disaccharide **8** in good yield.

With the disaccharide ligand **8** in hand, we carried out the synthesis of CS-E glycodendrimers **6** and **7** and the monovalent compound **5** (Scheme 2). First, we prepared disaccharide **5** by Cu^I catalysed cycloaddition (CuAAC) of azide-functionalized **8** and propargyl alcohol. This monovalent ligand, containing the triazole ring, will be used for comparison purposes with the multivalent systems.[10] Next, we conjugated ligand **8** and dendritic core **19** *via* a CuAAC reaction using the reaction conditions previously optimized in our lab for this type of conjugation: the reaction mixture was stirred at room temperature overnight in the presence of $CuSO_4$, tris(benzyltriazolylmethyl) amine (TBTA), and sodium ascorbate in a DMSO/PBS buffer mixture. After treatment with QuadraSil mercaptopropyl (MP) resin to remove the Cu catalyst and purification by size exclusion and ion-exchange chromatography using a Sephadex LH-20 gel and Dowex Na^+ resin, respectively, trivalent glycodendrimer **6** was obtained in good yield. The structure of compound **6** was confirmed by mass spectrometry and NMR analysis. Following our previously reported synthetic approach,[11] we also prepared the second-generation glycodendrimer **7**, displaying **9** copies of the CS-E disaccharide ligand. Thus, the cycloaddition reaction between disaccharide **8** and alkyne-functionalized dendritic core **20** afforded dendron **21** in moderate yield. Replacement of the chloro by an azido group at the focal position was accomplished by using sodium azide at 60 °C for 4 days providing compound **22**. Finally, this glycodendron **22** was conjugated to the alkyne-functionalized dendritic core **19**, using $CuSO_4$·$5H_2O$, sodium ascorbate and TBTA, to give the desired nonavalent system **7**. In this case, as described previously,[11] an additional purification step, using an Amicon Ultra-4 ultrafiltration device, was required to completely remove the remaining starting glycodendron **22**. The structure of glycodendrimer **7** was confirmed by NMR and MALDI-Tof mass spectrometry. In the latter case, the formation of a 1 : 1 complex between **7** and the synthetic, positively charged $(Arg\text{-}Gly)_{15}$ peptide was detected.[11]

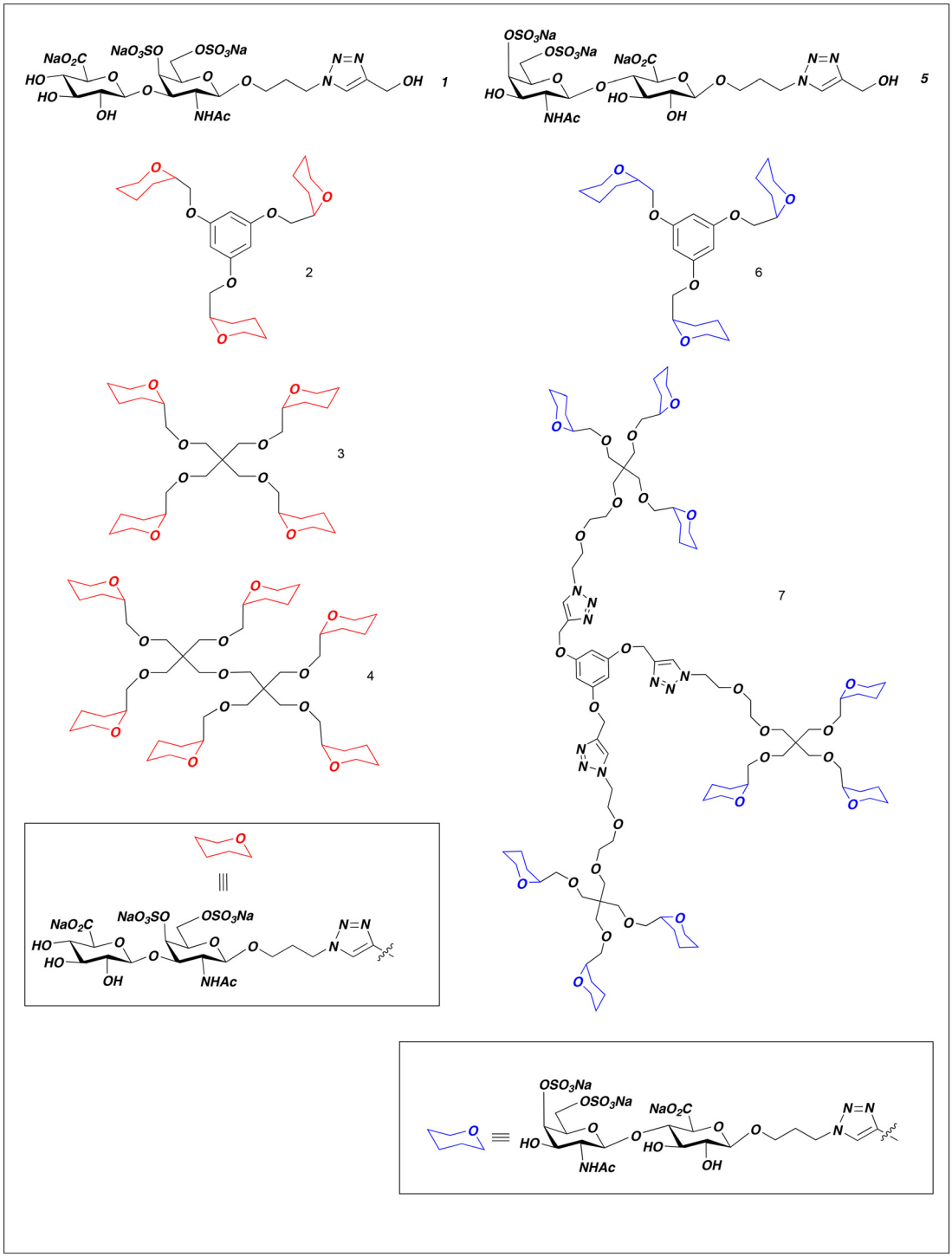

Fig. 1 Formulae of compounds **1–7**.

NMR analysis

We performed NMR analysis of the conformation of the derivatives shown in Fig. 1 and conducted an additional study using NMR transient methods with the corresponding receptor, in this case, langerin. This allowed us to analyze the conformation of the ligand first isolated and second in the complex.[10,11,18] In all cases, NMR analysis of free compounds was done using the same buffer and conditions, temperature, and concentration as those used in the presence of langerin to avoid potential bias due to the buffer composition. The presence of Ca^{2+} has been proposed to be essential for the for-

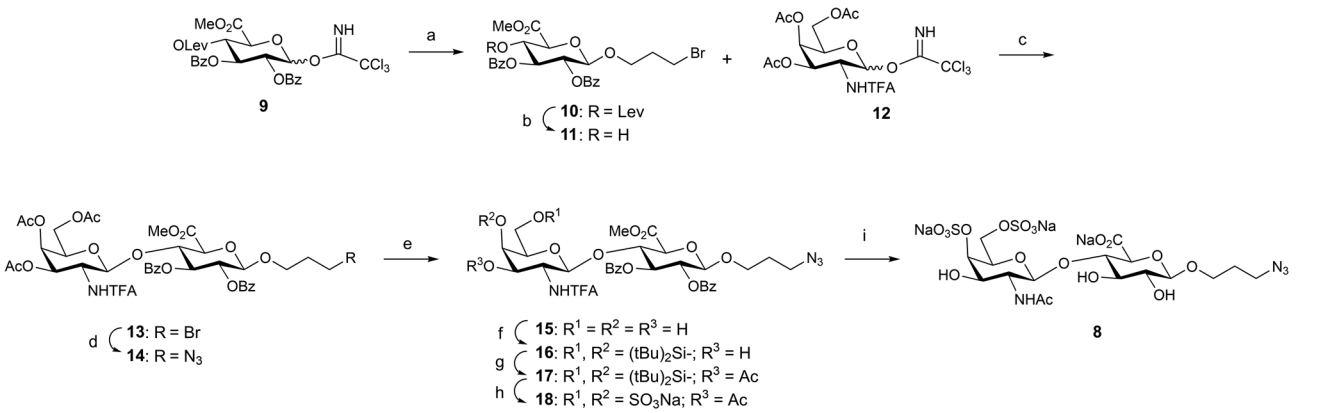

Scheme 1 Reagents and conditions: (a) 3-bromo-1-propanol, TMSOTf, CH_2Cl_2, 0 °C, 54%; (b) $NH_2NH_2{\cdot}H_2O$, Py/AcOH, CH_2Cl_2, 90%; (c) TMSOTf, CH_2Cl_2, 0 °C, 83%; (d) NaN_3, DMF, 98%; (e) *p*-TsOH, CH_2Cl_2/MeOH, 67%; (f) $tBu_2Si(OTf)_2$, Py, 76%; (g) Ac_2O, Py, DMAP, 99%; (h) $(HF)_n{\cdot}$Py, THF, 0 °C; $SO_3{\cdot}Me_3N$, DMF, 100 °C, MW, 30 min, 81%; and (i) NaOH, MeOH; Ac_2O, MeOH/H_2O, Et_3N, 78%. TMSOTf = trimethylsilyl trifluoromethanesulfonate; DMAP = 4-dimethylaminopyridine; and TFA = trifluoroacetyl.

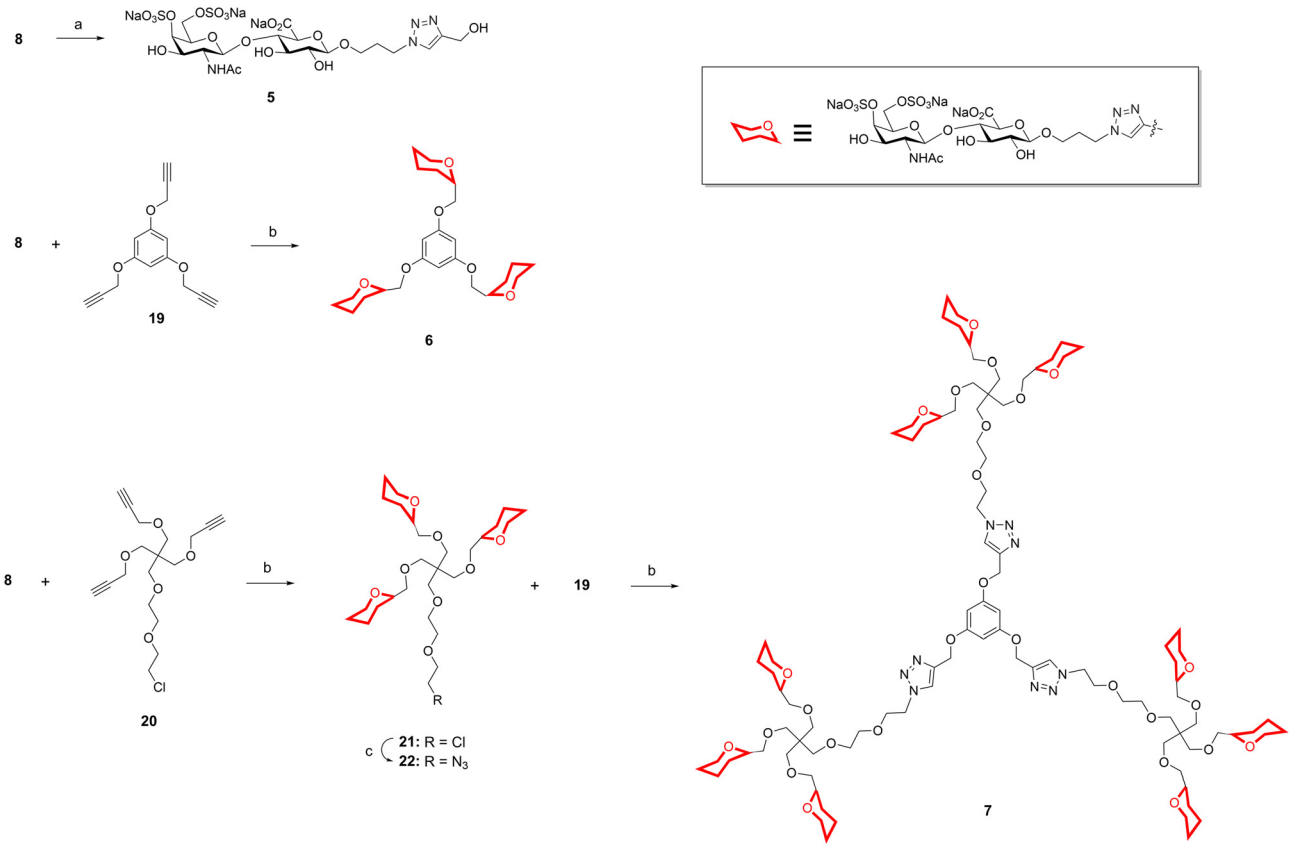

Scheme 2 Reagents and conditions: (a) propargyl alcohol, $CuSO_4{\cdot}5H_2O$, sodium ascorbate, TBTA, DMSO/PBS buffer, room temperature, overnight, 90%; (b) $CuSO_4{\cdot}5H_2O$, sodium ascorbate, TBTA, DMSO/PBS buffer, room temperature, overnight, 79% (for **6**), 46% (for **21**), 49% (for **7**); and (c) NaN_3, DMSO, 60 °C, 4 days, 85%. PBS = phosphate buffered saline.

mation of complexes between oligosaccharides and langerin by coordination with the terminal hydroxyl groups of the carbohydrate in a well-defined octahedral mode at the binding site.[4]

Free compounds

We investigated the structural characteristics of compounds with 1, 3, 4, and 6 branches, each containing glucuronic acid

at the non-reducing end (compounds **1**, **2**, **3**, and **4**). Additionally, we studied the corresponding compounds featuring the reverse disaccharide GalNAc–GlcA (compounds **5** and **6**). Detailed assignments and coupling constants can be found in Tables S1 and S2 of the SI.

The conformations exhibited coherence across the series. For compounds **1–4**, the ring conformations were consistent with a $^4C_1$ chair for both GlcA and GalNAc. This observation is supported by the observed coupling constants ($^3J_{HH}$) and by the Nuclear Overhauser Effect (NOE) between intraring protons in an axial disposition. The latter corresponds to the distance obtained by quantification of the NOE in a $^4C_1$ chair. The interglycosidic linkages in all cases indicated an *exo*-$\hat{\Phi}$/*syn*-Ψ disposition. The structure of the oligosaccharides with the alternative sequence (GalNAc–GlcA) was also analyzed. In this case, we found that **5** and **6** share the same structural features as the alternative disaccharide: the ring conformations were both in the $^4C_1$ chair and the glycosidic linkages were also in an *exo*-$\hat{\Phi}$/*syn*-Ψ disposition.

Consequently, the spatial arrangement of the disaccharide GlcA–GalNAc for compounds **1–4** was found to be similar to that of GalNAc–GlcA for compounds **5** and **6**, all exhibiting an *exo*-$\hat{\Phi}$/*syn*-Ψ arrangement. Additional data obtained from MD simulations are provided below.

The connecting regions with the triazole were compatible with free rotation of the aliphatic chain. This segment exhibited greater flexibility than the disaccharide. As expected, the larger anisotropy between the methylene protons was observed for the pair closest to the anomeric position.

The spectra exhibited remarkable similarity across the series due to the analogous components, except for the significant alterations that were noted upon the incorporation of an aromatic ring in compounds **2** and **6**. Distinctions in diffusional properties were utilized to discriminate between these compounds. A notable variation was observed in the NOE behavior, transitioning from a nearly null NOE in smaller molecules (**1** and **5**) to a negative NOE in larger ones (**2–4** and, **6**); see Fig. 2.

Complexes with langerin

In the preparation of complexes, molar ratios of langerin to the ligand were set as 1 : 12.5 (**1**), 1 : 25 (**2**), 1 : 50 (**3**), 1 : 50 (**4**), 1 : 25 (**5**), and 1 : 25 (**6**). Broadening of signals was observed, attributed to the formation of transient complexes. Notably, the buffer conditions used for experiments on free compounds mirrored those employed for transient experiments, ensuring consistent ionic strength effects on correlation times. The NOESY experiments in the presence of langerin, 20–80 μM, supported the same conformation and glycosidic linkage geometry as observed in the free state for all the compounds. Compound **1** served as the canonical example for transferred NOESY experiments. In the absence of langerin, the NOESY peaks were weak, prompting the use of transverse ROESY to avoid the zero-crossing region, which yielded peaks with signs opposite to the diagonal (see Fig. 2a). This behavior corresponds to a small–medium sized molecule tumbling regime. In the presence of langerin (see Fig. 2f) the sign changes towards the standard for large molecules. The NOESY cross-peak sign for the triazole of compound **1** in the presence of langerin corresponded to that of a small molecule, likely due to segmental flexibility with the triazole end tumbling in the small molecule regime.

Further NOESY and EASY-ROESY experiments with langerin (20–40 μM) confirmed that sugar rings and glycosidic linkage conformations of the disaccharides remained compatible with their free-state structure. For trimer **2**, tetramer **3**, and hexamer **4**, linewidth increment in cross-peaks indicated complex formation. Not surprisingly, **5** did not show any sign of binding in the presence of 4.0 mM Ca^{2+} likely because it lacks the terminal *cis*-diequatorial hydroxyl group disposition that is needed for Ca^{2+} chelation. As expected, in the absence of Ca^{2+} there was no evidence of binding in both cases **1** and **5**. Trimers **2** and **6** showed indications of complex formation with an increase in the intensity of cross peaks of the central moieties. However, the crosspeak intensities of **3** and **4** were already large in the free state and are not conclusive. This was the reason why we did not carry out these experiments with the larger nonavalent **7**.

STD-NMR experiments[19] were used to construct magnetization transfer growth curves (Fig. 3), which were instrumental in determining initial growth rates (STD_0). The obtained STD_0 values were then used to generate maps of the transfer of magnetization independent of relaxation (Fig. 3).[20]

The STD growth curves of compound **1** revealed the interaction at the lectin site, with two hydroxyl groups in a di-equatorial disposition, completing the coordination sphere of the Ca^{2+} atom (Fig. 3). This coordination pattern has been previously observed for heparin trisaccharides, consistently using the hydroxyl groups at 3 and 4 positions of the non-reducing end sugar for Ca^{2+} coordination.[21] In addition, in **1**, another pair of *trans*-di-equatorial hydroxyl groups in positions 2 and 3 also receives significant levels of magnetization.

In trimer **2**, a different binding mode was suggested by the greater impact of the aromatic core in the transfer of magnetization, implying an alternative binding orientation. The reliability of the STD initial rate method was underscored, ensuring unbiased results despite potential variations in relaxation rates. The observed STD values correlated with larger binding, aligning with previous findings when testing these compounds against midkine.[10]

In the case of compound **3**, a new binding site was unveiled through epitope mapping, with the most affected signal corresponding to proton 4 of the galactosamine ring, providing direct evidence of a previously unknown binding site. Compound **3** exhibited a weaker STD_0 value, less than 1%, further supporting the discovery of a new binding site. The overlap between the H4 and the water signal makes us check by varying the temperature to 278 K to assure the presence of this signal (see the SI).

Results for compound **4** were indicative of strong spin diffusion along the ligand signals, likely attributable to the large molecular size of the ligand and consequent long corre-

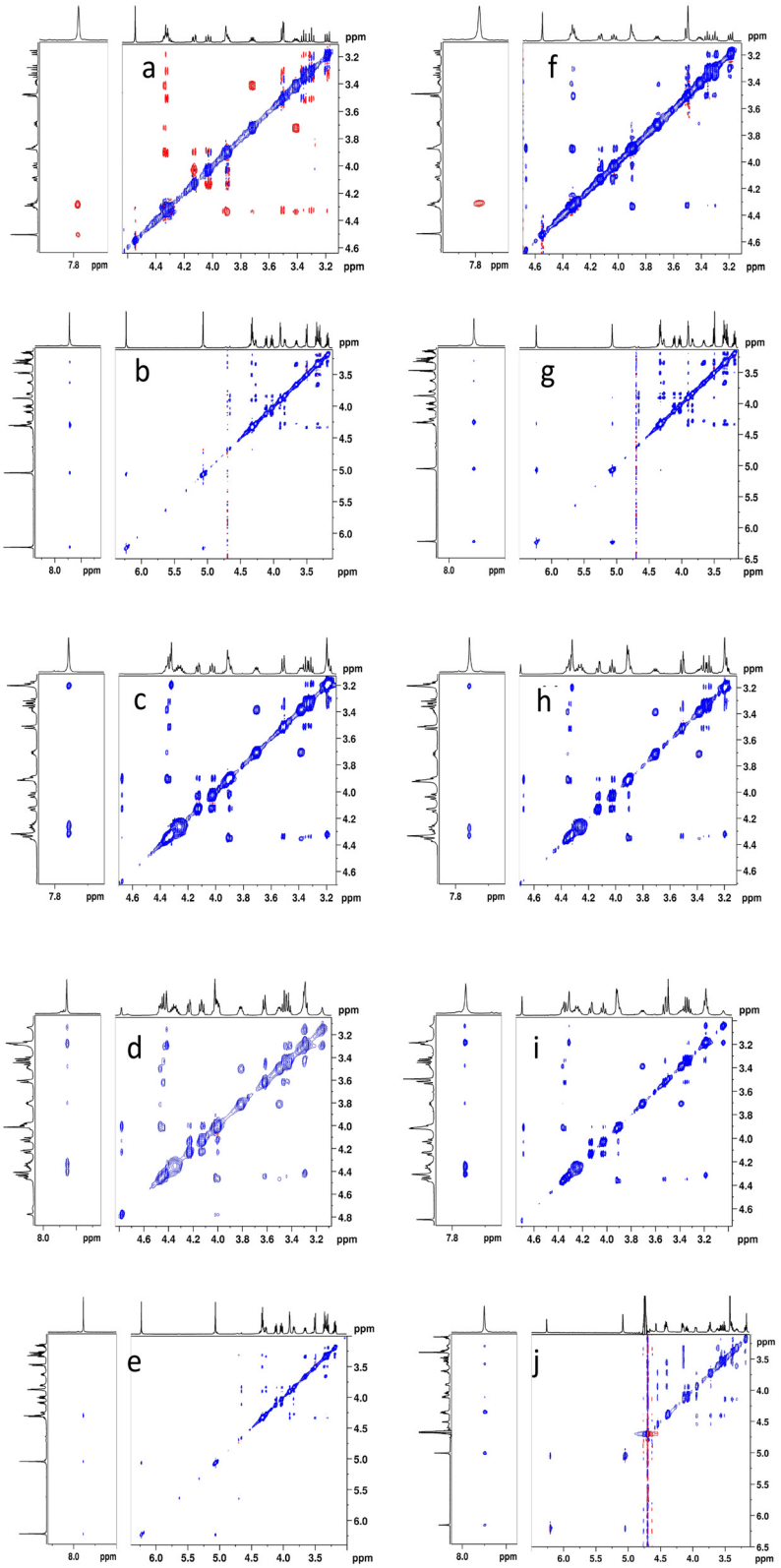

Fig. 2 Transversal ROESY (a) and NOESY (b–j) experiments at mixing time of 300 and 500 ms for **1**–**4** and **6** in the absence (a–e) NOESY and in the presence of langerin (f–j) transferred NOESY, using the same buffer at 298 K, (**1** a and f, **2** b and g, **3** c h, **4** d and i, and **6** e and j).

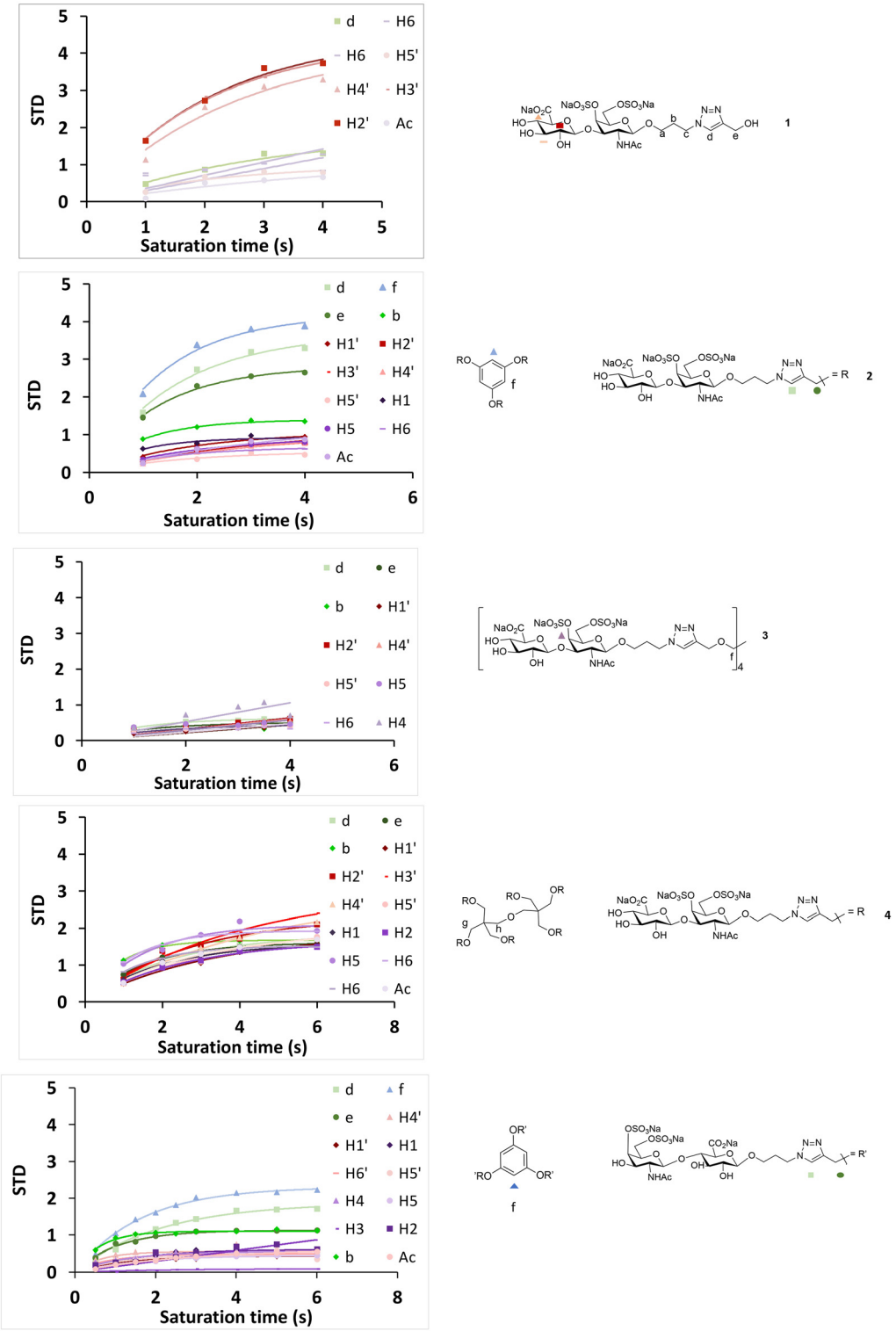

Fig. 3 STD growth curves of **1**–**4** and **6** and formulas showing epitope mapping.

lation time. However, this spin diffusion effect hindered further detailed analysis.

When we attempted to reproduce the binding experiments using a mixture of langerin and **5** in a 1 : 20 ratio and in the presence of Ca^{2+}, neither transferred NOESY nor STD provided evidence of binding, as for compound **1**. Specifically, no NOE peak sign changes or detection of peaks in the STD-NMR were detected (see Fig. 4). All the attempts to modify the experi-

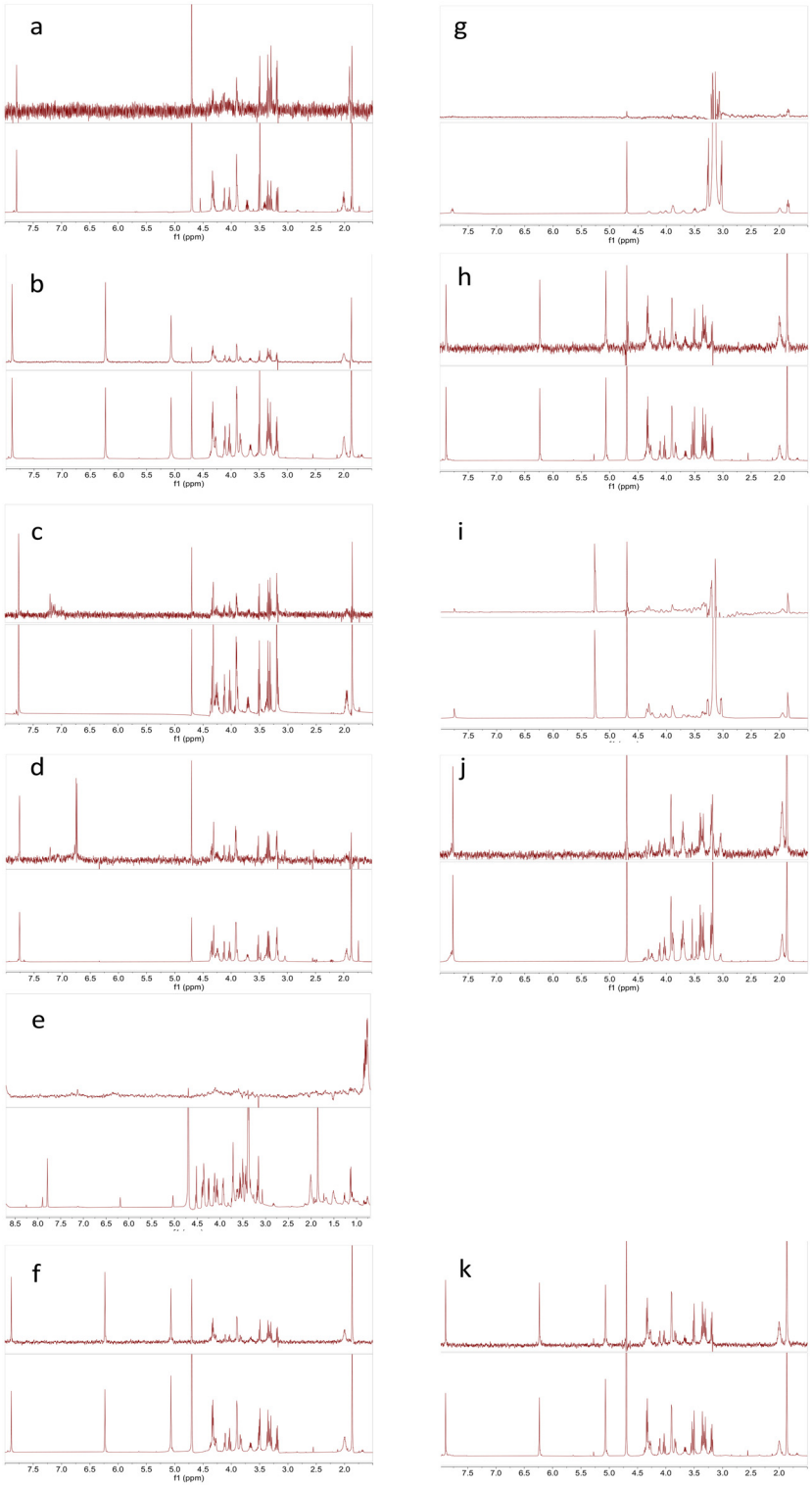

Fig. 4 STD-NMR experiments at 288 K in the presence of Ca^{2+}: (a) **1**; (b) **2**; (c) **3**; (d) **4**; (e) **5** and (f) **6** in the absence of Ca^{2+}: (g) **1**; (h) **2**; (i) **3**; (j) **4**, and (k) **6**. (bottom) Reference; (top) STD spectra.

mental conditions, such as a decrease in temperature to favor the hypothetical formation of a weak complex, were unsuccessful. Thus, it can be concluded that **5** did not bind to langerin as can be expected. This can be explained by the absence of a terminal *trans*-diequatorial hydroxyl arrangement responsible for Ca^{2+} binding needed for the Ca^{2+} interaction in the carbohydrate binding pocket. Notably, the disaccharide 6-SO_4-Galβ1-4GlcNAc has been reported as a langerin ligand; however, in

the complex structure the interaction between Ca^{2+} and the hydroxyl in **4** is prevented by the presence of SO_4^-.[4]

Conversely, compound **6** showed some signs of binding in STD experiments mainly from the aromatic peaks which appeared in an emptier spectral region (Fig. 4). The epitope map is very similar to that of **2**. This supports the existence of a new binding site for the central aromatic moiety common to **2** and **6**.

To further investigate langerin binding, STD experiments were recorded in the absence of Ca^{2+}, by adding deuterated EDTA (5 mM) to the previous STD samples to sequester the Ca^{2+} ions from the binding pocket where the *trans*-diequatorial hydroxyl groups coordinate with Ca^{2+} in an octahedral arrangement. This method has been used previously with trisaccharides that model the regular region of heparin.[21] Binding was abolished in the absence of Ca^{2+} in the lectin site, confirming, as in the case of heparin trisaccharides, that Ca^{2+} is necessary for interaction.[21] The same effect was observed for the case of **1**, compare Fig. 4 panels (a) and (g). Therefore, we propose a similar binding mode to the one described for heparin: an octahedral cage that stabilizes the Ca^{2+} ion in the presence of two hydroxyl groups from adjacent positions in the GlcA residue. Consistent results were obtained for **5**, which did not show binding even in the presence or absence of Ca^{2+}, suggesting that the presence of terminal hydroxyl groups is necessary for the interaction with the Ca^{2+} binding site of langerin.

However, when the same experiment was performed with the rest of the compounds, we obtained STD signals compatible with binding in the absence of Ca^{2+} (Fig. 4). The epitope mapping obtained from the STD growth curves for **2** and **6** suggested a predominant role of the central phenyl moiety very similar to that in the presence of Ca^{2+}. Thus, the interaction *via* terminal hydroxyl groups with Ca^{2+} is not mandatory for the formation of the complexes.

For compounds **3** and **4**, the STD results in the absence of Ca^{2+} (Fig. 4c, i; d, j) indicated an alternative binding mode not yet substantiated, **3**, or masked by a severe spin diffusion, **4**.

DOSY

Diffusion-ordered spectroscopy (DOSY) experiments were conducted to characterise the synthetic multivalent chondroitin sulfate E (CS-E) derivatives, focusing on their diffusion behaviour and interaction dynamics with the langerin receptor. Due to the structural similarities among the synthesised glycodendrimers, DOSY provided an essential means of their differentiation, complementing conventional chemical shift analyses.

Initial DOSY experiments performed on free compounds demonstrated diffusion coefficients corresponding to their molecular sizes (Fig. 5a), confirming the expected trend: larger dendrimers exhibited progressively lower diffusion coefficients.

A quantitative analysis of DOSY data allowed the calculation of diffusion coefficients and hydrodynamic radii (rHr_HrH), confirming size-dependent trends (Table 1). Detailed DOSY results for compound **3** are illustrated in Fig. 6, with additional data provided in the SI (Fig. S11–S13).

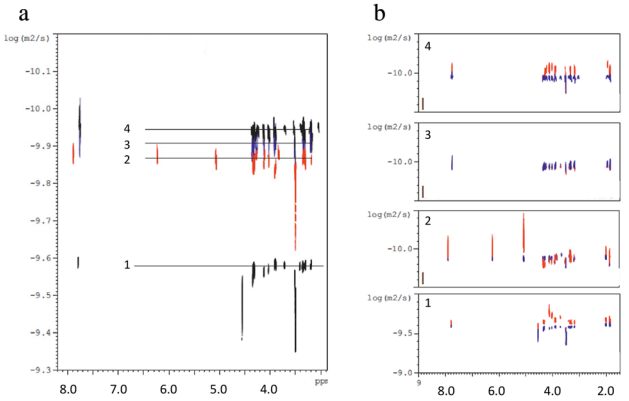

Fig. 5 (a) Superimposition of individual DOSY experiments of **1**, **2**, **3** and **4**. (b) Superimposition of individual DOSY experiments in the presence (red) and in the absence (blue) of langerin of **1**, **2**, **3**, and **4** (1 : 12.5; 1 : 25; 1 : 50 and 1 : 50).

Table 1 TRAln diffusion coefficients (D) and hydrodynamic radii (r_H) at 298 K in D_2O

Compound	D_{av} (10^{-9} m^2 s^{-1})	r_H [a] (Å)
1	0.56 ± 0.01	3.85 ± 0.1
2	0.25 ± 0.02	8.6 ± 0.2
3	0.23 ± 0.01	9.4 ± 0.2
4	0.16 ± 0.01	13.5 ± 0.1

[a] The viscosity η used in the Stokes–Einstein equation was taken from Perry's Chemical Engineers' Handbook 8th Edition (https://www.knovel.com) and is 0.98086×10^{-3} kg m^{-1} s^{-1}.

Upon langerin addition, significant changes in diffusion coefficients were observed, indicating a reduction in dendrimer mobility due to protein interaction and concomitant mass changes (Fig. 5b). Qualitatively, the deviations in diffusion coefficients indicated deceleration in the hydrodynamic motions of the dendrimers due to the interaction with the protein (Fig. 5b). The degree of retardation is a function of the number of interacting disaccharides and of the presence of the aromatic central core of **2**, which is above the trend.

When a single DOSY experiment was performed on a mixture of all compounds (**1–4**), the results were consistent with the relative sizes of the ligands (Fig. 7). In the range of chemical shifts from 7.80 to 8.05 ppm we were able to observe different signals for the triazole protons allowing the determination of the diffusion coefficients of each compound in the mixture allowing the determination of distinct species **1–4** in solution.

The diffusion coefficients of the free compounds correlated well with their molecular volumes, reinforcing the expected trends. However, upon langerin addition, notable variations were observed for compounds **1**, **2**, **3** and **4**, indicating reduced mobility due to protein binding (Table 2, ranging from 0.18 to 0.09×10^{-9} m^2 s^{-1}).

In summary, the observed diffusion coefficients of the free compounds aligned well with their respective volumes, corro-

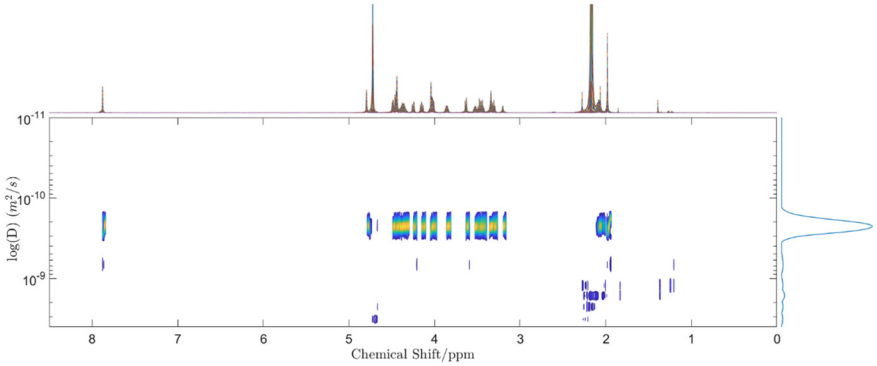

Fig. 6 SILT-DOSY experiment for compound **3**. The estimated diffusion coefficient is 0.23 ± 0.01 (10^{-9} m^2 s^{-1}) with a hydrodynamic radius (r_H) of 9.4 ± 0.2 (Å).

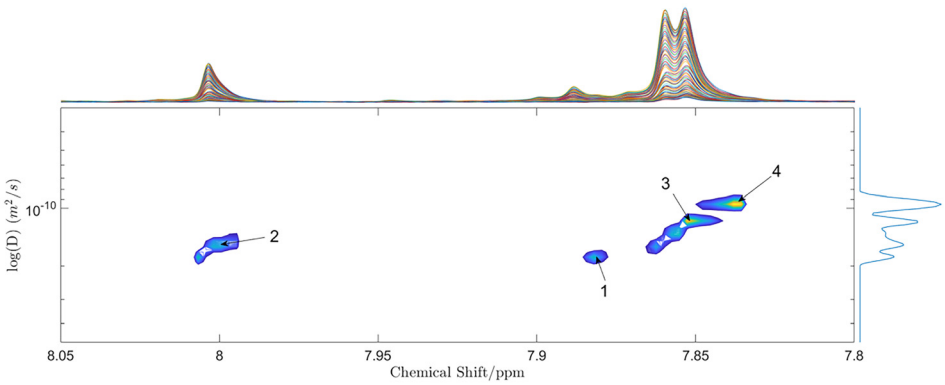

Fig. 7 SILT-DOSY experiment for the **1**, **2**, **3** and **4** mixture. The range of chemical shifts observed belong to the triazol protons between 7.80 and 8.05 ppm.

Table 2 Diffusion coefficients (D) and hydrodynamic radii (r_H) of a mixture of compounds **1**, **2**, **3** and **4** in the presence of langerin at 288 K in D_2O

Species	D (10^{-9} m^2 s^{-1})	r_H [a] (Å)
1	0.18 ± 0.01	12.0 ± 0.1
2	0.15 ± 0.01	14.4 ± 0.1
3	0.12 ± 0.01	18.0 ± 0.1
4	0.09 ± 0.01	24.0 ± 0.1

[a] The viscosity η used in the Stokes–Einstein equation was taken from Perry's Chemical Engineers' Handbook 8th Edition (https://www.knovel.com) and is 0.98086 × 10^{-3} kg m^{-1} s^{-1}.

borating the expected trends. Upon langerin interaction, diffusion coefficients decrease, with a notable variation for compounds **1**, **2**, **3**, and **4**, consistent with protein binding and complex formation. This effect was more pronounced for compound **2** (Fig. 5b), suggesting the participation of the central linker.

Ongoing studies with binary and ternary mixtures at various compound ratios aim to elucidate the complex interaction dynamics and equilibrium states. Preliminary findings indicate a dynamic equilibrium between the ligand and receptor in solution, with the ligand consistently in excess. This observation contrasts with complementary techniques, such as SPR, which can extend beyond the equimolar range and multiple bound ligand complexes have been detected.

Molecular dynamics

We have performed molecular dynamics simulations to complement the NMR experimental data. MD simulations were performed using the AMBER software package[22] with GLYCAM06[23] parameters. Initial MD runs were performed for **1**, **2**, and **3** followed by a similar study with some of the alternative compounds (**5** and **6**), followed by simulations in implicit water and Periodic Boundary Conditions (PBCs).[24] From the runs, we extracted time-averaged experimental magnitudes as $^3J_{HH}$ or interprotonic distances and compared them with the experimental ones (see the Experimental part and SI for a large description). First, we calculate the puckering angles for the rings (see the SI). They were consistent with a stable $^4C_1$ conformation for both rings along the whole trajectory. In all cases, calculated puckering agrees with that experimentally observed, and they were stable along the whole trajectory, independent of the disaccharide sequence. The complementary disaccharide found in **5–6** behaves similarly with

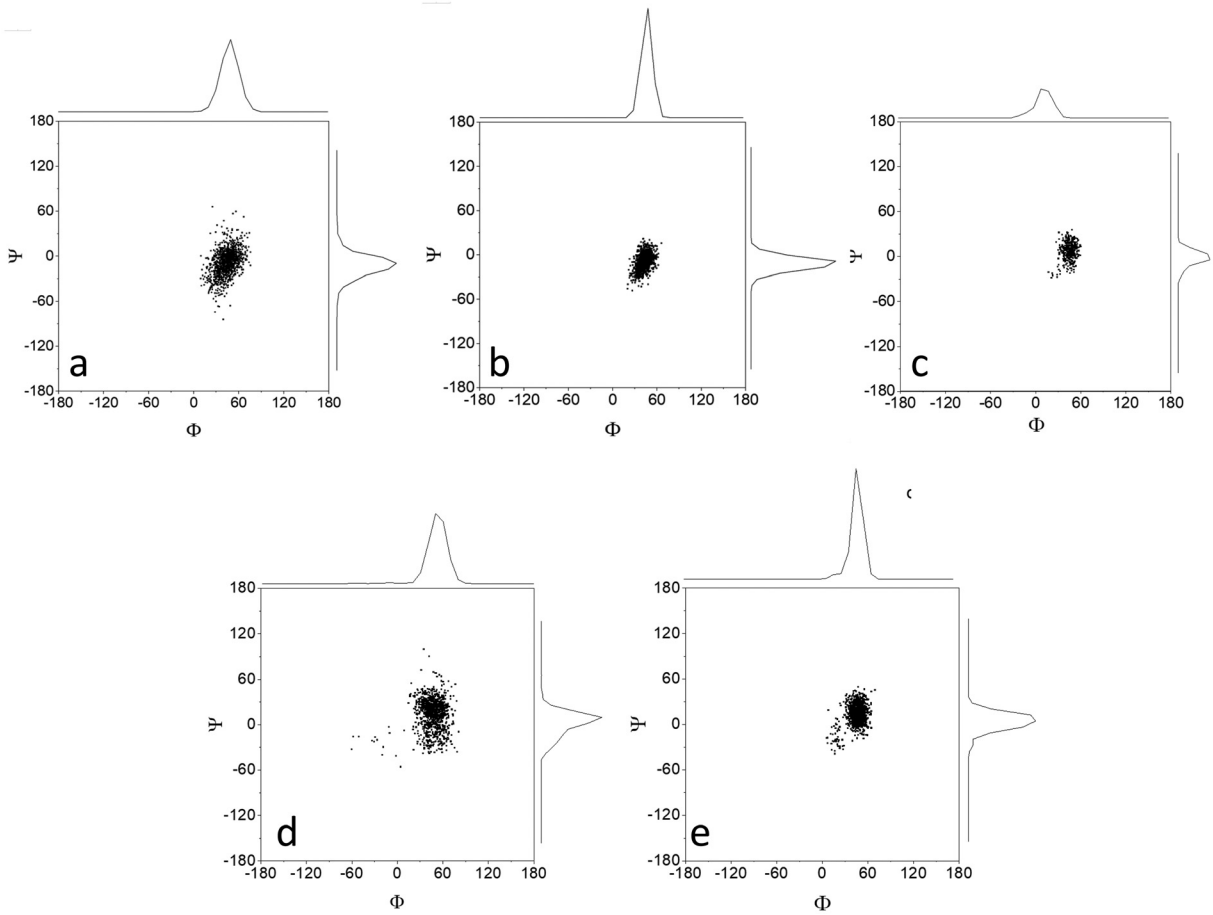

Fig. 8 Interglycosidic dihedral angle plots of compounds (a) **1**, (b) **2**, (c) **3**, (d) **5** and (e) **6**.

ring conformations in $^4C_1$. The glycosidic linkage conformation is also similar for both types of disaccharides, corresponding to an *exo-Φ*/*syn-Ψ* conformation very similar for both types of linkages (Fig. 8). This is in agreement with the experimental observations (the NOE and torsional angles obtained from $^3J_{HH}$).

Finally, in all cases, the linker chain connecting the disaccharides with the dendritic core is more flexible than the rest of the molecule, leading to the averaging of methylene signals. Only the methylene closer to the anomeric position exhibits diastereotopicity, appearing at two different chemical shifts due to its proximity to a chiral center. Thus, the mobility of the molecules can be described as a rigid part, the disaccharide, and a flexible region, the linker.

Conclusions

NMR spectroscopy combined with molecular modelling has been used to analyze the interaction between multivalent CS-E disaccharides and langerin. The disaccharides exhibit two alternative sequences: GlcA–GalNAc and GalNAc–GlcA. The rest of the molecule includes a linker and a central core to provide multivalency. NMR structural analysis of all compounds in their free states indicates that the central core does not affect the three-dimensional structure of the terminal disaccharides. Regardless of the sequence and linkers, all sugars are in the $^4C_1$ conformation with glycosidic linkages in the *exo-Φ̂*/*syn-Ψ* disposition. Upon interaction with langerin, the structural characteristics of the ligands, obtained from NMR analysis, remain the same as those in the free compounds. Consequently, the structures of the terminal disaccharides (in both the free and bound states) mirror those of the natural CS-E disaccharide repeating units.

Interaction studies *via* transfer-NOESY NMR experiments confirm that the carbohydrate moieties retain their geometry upon binding, supporting the paradigm that ligand preorganization reduces the entropic penalty associated with ligand binding.

STD-NMR experiments were recorded for **1–6**. Compounds **1–4** feature three hydroxyl groups in a *trans*-diequatorial disposition at positions 4, 3 and 2 at the non-reducing end sugar that were tailored for the interaction *via* the Ca^{2+} atom of langerin by fulfilling the octahedral coordination around the calcium atom at the binding site.[25] Compound **1** interacts with Ca^{2+} at this site, previously described for heparin trisacchar-

ides.[21] In the absence of Ca^{2+}, the interaction between **1** and langerin does not occur, consistent with prior observations.[21] In contrast, compound **5**, lacking terminal hydroxyls, showed no detectable binding in the presence or absence of Ca^{2+}. Interestingly, compounds **2** and **6** were also capable of interacting with langerin but using the central aromatic core, as can be deduced by the STD peaks that correspond to the central aromatic moiety (see Fig. 3). The presence of Ca^{2+} is irrelevant in both cases, and the evidence of binding of **6** that has no hydroxyl arrangement for Ca^{2+} mediated binding suggests that there should be another binding site for **2** and **6**.

Compounds **3** and **4** also interact with langerin in both Ca^{2+} dependent and independent manners. Although strong spin diffusion hindered a detailed STD analysis of **4**, an alternative STD pattern was observed for **3** where the internal GalNAc residue holds the maximum STD peak.

In summary, epitope mapping *via* STD reveals multiple binding sites, including those independent of Ca^{2+}, such as aromatic–aromatic interactions observed in compounds **2** and **6**, or others previously reported.[25] Moreover, multivalency introduces the possibility to interact with alternative binding sites, potentially elucidating the variety of binding epitopes found within each series.

Overall, the introduction of multivalency expands the repertoire of potential binding sites, providing new perspectives on CS-E disaccharide interactions with langerin. These findings contribute to a deeper understanding of carbohydrate–protein multivalent interactions, paving the way for the development of novel therapeutic strategies targeting langerin and related C-type lectin receptors.

Experimental

NMR

NMR experiments were performed using a 600 MHz Bruker Avance III instrument, equipped with a cryoprobe (QCI Cryo 5 mm (1H/19F 15N/13C) for ^{1}H, ^{15}N, ^{13}C, and ^{19}F, with 2H decoupling) at 288 K in 3 mm NMR tubes of 1.5 mM ligand in 150 mM NaCl, 30 mM Tris-d_{11} buffer, with added 4.0 mM $CaCl_2$ at pH 8. We have assigned the ^{1}H and ^{13}C spectra using the standard methodology based on ^{1}H and ^{13}C NMR methods at natural abundance. First, we used pure D_2O to optimize the experimental conditions and then in the buffer used for the interaction with langerin to have more accurate data in the media where the interactions would be measured. Logically, upon salt addition, the signals become broader, increasing the probability of signal overlapping.

NMR experiments were performed using the manufacturer's pulse sequences. 1D, 1D-TOCSY or 1D-NOESY, 2D COSY with double quantum filter with pulsed field gradient for coherence selection, and TOCSY with a DIPSI2 sequence in the mixing period were used;[26] NOESY was implemented in the phase sensitive mode with one or two 180° pulses flanked with gradients in the mixing time.[27] Both TOCSY and NOESY were performed with a *z*-filter to suppress interferences of zero quantum coherence.[28] The last dipolar coupling experiments (for 5 and 6) were performed using the EASY-ROESY sequence proposed by Thiele[29] as it allows the extraction of distances without making any assumption on the correlation times of interprotonic vectors.

NOESY experiments were preferentially performed using non-uniform sampling at 100% to minimize periodic interferences from the environment due to thermal instability. ^{13}C-HSQC was generally performed using echo/antiecho or TPPI acquisition with an increase of sensitivity, Chirp 180° pulses in ^{13}C, and gradients during back inept, obtained from the manufacturer's pulse sequence library.

Coupling constants were calculated from the splitting of the signals in monodimensional 1D, 1D-TOCSY or 1D-NOESY. Interprotonic distances were calculated from NOE data using the ISPA approach with the initial growth rates of the dipolar rate constant by fitting the growth curve of the NOE *versus* the mixing time to a monoexponential equation employing mixing times from 0.15 to 0.8–1.2 s according to the known procedure recently reviewed by others and us using the PANIC approach when possible.[30,31] Distances from EASY-ROESY were estimated from the growth rates at various tilted angles.

STD-NMR experiments were performed using home-written sequences with solvent suppression using watergate or excitation sculpting sequences. In order to avoid the influence of the proton relaxation rates, we used STD_0 calculated from the evolution of the STD with the saturation time (t_{sat}), fitted to the equation $\text{STD-AF}(t) = a(1 - \exp(-bt))$, where parameter a represents the asymptotic maximum of the STD build-up curve (STD_{max}), b is a rate constant related to the relaxation properties of a given proton that measures the speed of the STD build-up (k_{sat}), and t is the saturation time (t_{sat}). Thus, the STD_0 values were obtained as the product of the ab coefficients.[32,33]

DOSY experiments were performed using the standard sequences from the Bruker library (ledbpgp2s)[33] using the Δ and δ values that were fixed as 150–100 ms and 1.2–1.6 ms. The gradient strength was increased linearly from 2 or 20%, if excessive HDO was observed to optimize the receiver gain, to 95%. The recovery delay was always set to 2 s.

The number of scans per increment was 32 and typical experimental times were around 45 min for free compound NMR samples and 90 min for the mixture NMR sample. All the experiments were conducted without spinning at 288.1 ± 0.1 K. The diffusion measurements were carried out using the stimulated echo with bipolar pair pulses including a final longitudinal-eddy-current delay (BPP-LED).[33] A smoothed rectangular shape (SMSQ) was used for the gradient pulses and their strength varied automatically during the experiments as mentioned before. The D values were determined from the slope of the non-linear regression $\ln(I/I_0)$ *versus* G^2, according to the Stejskal–Tanner equation for SMSQ gradient pulses (eqn (1)),[34] where I/I_0 = observed spin echo intensity/intensity without gradients, G = gradient strength, Δ = delay between the midpoints of the gradients, D = diffusion coefficient, δ = gradi-

ent length, and τ = duration of the gradient recovery delay and the 180° pulse.

$$\ln\left(\frac{I}{I_0}\right) = (\gamma\delta)^2\left(\Delta - \frac{6.344\pi^2 - 207}{19.44\pi^2}\delta - \frac{\tau}{2}\right)D\frac{81}{100}G^2 \quad (1)$$

Determination of the *D*-values was performed by applying different algorithms. dART solutions were obtained using an algebraic reconstruction technique.[34] TRAIn solutions were obtained by the use of the algorithm provided by Xu *et al.*,[35] with an alpha parameter set to 1.05. LMS fittings were performed with the help of the DiffAtOnce package.[36] DOSY NMR spectra were recorded with the alternating direction sparse and low rank unmixing algorithms (ADSpLRU) reported by Giampouras *et al.*[37] and applied for the first time to the resolution of DOSY maps by Yuan *et al.* called SILT-DOSY.[38]

Molecular dynamics

MD was performed using explicit water methodology with AMBER 20.[22,39] We used GLYCAM-Web[39] with GLYCAM06j 23 force field parameters adapted to include non-carbohydrate substituents to construct the topology and parameters. For atoms not included in GLYCAM we used the ff19SB library.

This procedure was described, tested, and optimized by us with a library of heparin trisaccharides.[31] The parameters for the substituents that were not included in GLYCAM06j-1 were taken from AMBER[22] standard libraries, and charges were obtained from GLYCAM.

Each of the models was immersed in a cube of pre-equilibrated TIP3P water molecules.

To equilibrate the system, we followed a protocol consisting of 10 steps.[40] Firstly, only the water molecules and ions were minimized. Then the system is heated to 300 K by a 3 ps MD simulation, allowing only water molecules and ions to move. Next, the whole system is minimized by four consecutive steps imposing positional restraints on the solute, with a force constant decreasing step by step from 20 to 5 kcal mol^{-1}. Finally, non-restraint minimization (100 steps) is carried out.

The production dynamics simulations were accomplished at a constant temperature of 300 K (by applying the Berendsen coupling algorithm[24] for temperature scaling) and constant pressure (1 bar). The particle mesh Ewald method[41] (to introduce long-range electrostatic effects) and periodic boundary conditions were also turned on. The SHAKE algorithm for hydrogen atoms, which allows using a 2.0 fs time step, was also employed with a 9 Å cutoff applied for Lennard-Jones interactions.

These MD simulations were performed with the pmemd module of Amber. The trajectory coordinates were saved every 0.5 ps. The data processing of the trajectories was done with the *ptraj* module of AMBER.

Conclusions

NMR spectroscopy combined with molecular modelling was used to analyze the interaction between multivalent CS-E disaccharides and langerin. The disaccharides exhibit two alternative sequences: GlcA–GalNAc and GalNAc–GlcA. The rest of the molecule includes a linker and a central core to provide multivalency. NMR structural analysis of all the compounds in their free state indicates that the central core does not affect the three-dimensional structure of the terminal disaccharides. Regardless of the sequence and linkers, all sugars are in the $^4C_1$ conformation with glycosidic linkages in an *exo*-$\hat{\Phi}$/*syn*-Ψ disposition. Upon interaction with langerin, the structural characteristics of the ligands obtained from NMR analysis remain consistent with those in the free compounds. Consequently, the structures of the terminal disaccharides (in both the free and bound states) mirror those of the natural CS-E disaccharide repeating units.

Interaction studies using transfer-NOESY NMR experiments confirm that the geometries of the carbohydrate moieties in the complexes align with those in their free states. This preorganization of the ligand diminishes the entropic cost associated with langerin binding.

We recorded STD-NMR experiments of **1–6**. Compounds **1–4** feature three hydroxyl groups in a *trans*-diequatorial disposition at positions 4, 3 and 2 in the non-reducing end sugar that were tailored for the interaction *via* the Ca^{2+} atom of langerin by fulfilling the octahedral coordination around the calcium atom at the binding site.[25] Compound **1** interacts with Ca^{2+} at this site, previously described for heparin trisaccharides.[21] In the absence of Ca^{2+}, the interaction between **1** and langerin does not occur, consistent with prior observations.[21] As can be expected, compound **5**, lacking terminal hydroxyls, showed no detectable binding in the presence or absence of Ca^{2+}. Interestingly, compounds **2** and **6** were also capable of interacting with langerin but using the central aromatic core, as can be deduced by the STD peaks that correspond to the central aromatic moiety (see Fig. 3). The presence of Ca^{2+} is irrelevant in both cases, and the evidence of binding of **6** that has no hydroxyl arrangement for Ca^{2+} mediated binding suggests that there should be another binding site for **2** and **6**.

Compounds **3** and **4** also interact with langerin in both Ca^{2+} dependent and independent manners. Although strong spin diffusion hindered the accurate STD analysis of **4**, an alternative STD pattern was observed for **3**, where the internal GalNAc residue holds the maximum STD peak.

In summary, epitope mapping *via* STD reveals multiple binding sites, including those independent of Ca^{2+}, such as aromatic–aromatic interactions observed in compounds **2** and **6**. Moreover, multivalency introduces the possibility of interacting with alternative binding sites, potentially elucidating the variety of binding epitopes found within each series.

Overall, the introduction of multivalency expands the repertoire of potential binding sites, providing new perspectives on CS-E disaccharide interactions with langerin. These findings contribute to a deeper understanding of carbohydrate–protein multivalent interactions, paving the way for the development of novel therapeutic strategies targeting langerin and related receptors.

Author contributions

Conceptualization: PMN, JLP, and FAC; data curation: MJGJ and SG; funding acquisition; PMN, JR, FF, and IF; investigation: MJGJ, SG, PDR, LR, and MT; methodology: SG; resources: PMN; software: FAC, MJGJ, and FAC; supervision: PMN, JLP, and IF; writing: FAC, MT, FF, and JR; writing review and editing: PMN and JLP.

Conflicts of interest

There are no conflicts to declare.

Data availability

Data supporting this article have been included in the SI: general synthetic procedures; synthesis and spectral data of the prepared compounds, NMR data for **1–6** (chemical shifts and coupling constants), STD growth curves in the presence and absence of Ca^{2+}, DOSY, and molecular dynamics trajectories. See DOI: **https://doi.org/10.1039/d5ob00845j**.

MD coordinates along the calculated trajectories in AMBER format are available upon request.

Acknowledgements

Financial support was provided by the Spanish Ministry of Science Innovation and Universities MCIN/AEI/10.13039/501100011033 (PGC2018-099497-B100, PID2020-118403GB-I00, and PID2021-125094NB-I00) and Junta de Andalucía (FQM-1303 and P20_00515). We would like to thank the BioInteraction Platform (BIP-cicCartuja, Seville) for NMR measurements. F. F. acknowledges the French Agence Nationale de la Recherche PIA for Glyco@Alps (ANR-15-IDEX-02) and the ANR PRCI LectArray 19-CE18-0019-01.

References

1 *Essentials of Glycobiology*, ed. A. Varki, R. D. Cummings, J. D. Esko, P. Stanley, G. W. Hart, M. Aebi, T. Kinoshita, D. Mohnen, N. H. Packer, J. H. Prestegard, R. L. Schnaar and P. H. Seeberger, Cold Spring Harbor Laboratory Press, Cold Spring Harbor, New York, 2022.
2 S. Perez, O. Makshakova, J. Angulo, E. Bedini, A. Bisio, J. L. de Paz, E. Fadda, M. Guerrini, M. Hricovini, M. Hricovini, F. Lisacek, P. M. Nieto, K. Pagel, G. Pairardi, R. Richter, S. A. Samsonov, R. A. Vives, D. Nikitovic and S. R. Blum, *JACS Au*, 2023, **3**, 628–656.
3 S. Ricard-Blum, R. R. Vivès, L. Schaefer, M. Götte, R. Merline, A. Passi, P. Heldin, A. Magalhães, C. A. Reis, S. S. Skandalis, N. K. Karamanos, S. Perez and D. Nikitovic, *FEBS J.*, 2024, **291**, 3331–3366.
4 H. Feinberg, M. E. Taylor, N. Razi, R. McBride, Y. A. Knirel, S. A. Graham, K. Drickamer and W. I. Weis, *J. Mol. Biol.*, 2011, **405**, 1027–1039.
5 E. Chabrol, A. Nurisso, A. Daina, E. Vassal-Stermann, M. Thepaut, E. Girard, R. R. Vivès and F. Fieschi, *PLoS One*, 2012, **7**, e50722.
6 M. J. García-Jiménez, S. Gil-Caballero, S. Maza, F. Corzana, F. Juárez-Vicente, J. R. Miles, K. Sakamoto, K. Kadomatsu, M. García-Domínguez, J. L. Paz and P. M. Nieto, *Chem. – Eur. J.*, 2021, **27**, 12395–12409.
7 M. Torres-Rico, S. Maza, J. L. de Paz and P. M. Nieto, *Org. Biomol. Chem.*, 2021, **19**, 5312–5326.
8 M. Jose Garcia-Jimenez, M. Torres-Rico, J. L. de Paz and P. M. Nieto, *Int. J. Mol. Sci.*, 2022, **23**, 3026–3032.
9 J. R. Miles, X. Wang, J. L. de Paz and P. M. Nieto, *Pharmaceuticals*, 2022, **15**, 496–516.
10 P. Dominguez-Rodriguez, J. J. Reina, S. Gil-Caballero, P. M. Nieto, J. L. de Paz and J. Rojo, *Chem. – Eur. J.*, 2017, **23**, 11338–11345.
11 P. Domínguez-Rodríguez, C. Vivès, M. Thepaut, F. Fieschi, P. M. Nieto, J. L. de Paz and J. Rojo, *Biomacromolecules*, 2020, **21**, 2726–2734.
12 N. S. Stambach and M. E. Taylor, *Glycobiology*, 2003, **13**, 401–410.
13 I. Herrera-Gonzalez, M. Thepaut, E. M. Sanchez-Fernandez, A. di Maio, C. Vives, J. Rojo, J. M. G. Fernandez, F. Fieschi, P. M. Nieto and C. O. Mellet, *Chem. Commun.*, 2022, **58**, 12086–12089.
14 K. Aït-Mohand, C. Lopin-Bon and J. C. Jacquinet, *Carbohydr. Res.*, 2012, **353**, 33–48.
15 P. Bindschadler, C. Noti, E. Castagnetti and P. H. Seeberger, *Helv. Chim. Acta*, 2006, **89**, 2591–2610.
16 M. Mar Kayser, J. L. de Paz and P. M. Nieto, *Eur. J. Org. Chem.*, 2010, 2138–2147.
17 C. Solera, G. Macchione, S. Maza, M. M. Kayser, F. Corzana, J. L. de Paz and P. M. Nieto, *Chem. – Eur. J.*, 2016, **22**, 2356–2369.
18 J. Rojo, M. P. Nieto and L. J. de Paz, *Curr. Med. Chem.*, 2022, **29**, 1173–1192.
19 B. Meyer and T. Peters, *Angew. Chem., Int. Ed.*, 2003, **42**, 864–890.
20 J. Angulo and P. M. Nieto, *Eur. Biophys. J.*, 2011, **40**, 1357–1369.
21 J. C. Munoz-Garcia, E. Chabrol, R. R. Vives, A. Thomas, J. L. de Paz, J. Rojo, A. Imberty, F. Fieschi, P. M. Nieto and J. Angulo, *J. Am. Chem. Soc.*, 2015, **137**, 4100–4110.
22 D. A. Case, T. E. Cheatham 3rd, T. Darden, H. Gohlke, R. Luo, K. M. Merz Jr., A. Onufriev, C. Simmerling, B. Wang and R. J. Woods, *J. Comput. Chem.*, 2005, **26**, 1668–1688.
23 K. N. Kirschner, A. B. Yongye, S. M. Tschampel, J. Gonzalez-Outeirino, C. R. Daniels, B. L. Foley and R. J. Woods, *J. Comput. Chem.*, 2008, **29**, 622–655.
24 H. J. C. Berendsen, J. P. M. Postma, W. F. van Gunsteren, A. DiNola and J. R. Haak, *J. Chem. Phys.*, 1984, **81**, 3684–3690.
25 L. Chatwell, A. Holla, B. B. Kaufer and A. Skerra, *Mol. Immunol.*, 2008, **45**, 1981–1994.

26 J. Cavanagh and M. Rance, *J. Magn. Reson.*, 1992, **96**, 670–678.
27 K. Stott and J. Keeler, *Magn. Reson. Chem.*, 1996, **34**, 554–558.
28 M. J. Thrippleton and J. Keeler, *Angew. Chem., Int. Ed.*, 2003, **42**, 3938–3941.
29 C. M. Thiele, K. Petzold and J. Schleucher, *Chem. – Eur. J.*, 2009, **15**, 585–588.
30 S. Macura, B. T. Farmer and L. R. Brown, *J. Magn. Reson.*, 1986, **70**, 493–499.
31 J. C. Munoz-Garcia, F. Corzana, J. L. de Paz, J. Angulo and P. M. Nieto, *Glycobiology*, 2013, **23**, 1220–1229.
32 J. Angulo, P. M. Enriquez-Navas and P. M. Nieto, *Chem. – Eur. J.*, 2010, **16**, 7803–7812.
33 D. H. Wu, A. D. Chen and C. S. Johnson, *J. Magn. Reson., Ser. A*, 1995, **115**, 260–264.
34 D. Sinnaeve, *Concepts Magn. Reson., Part A*, 2012, **40**, 39–65.
35 K. P. Xu and S. M. Zhang, *Anal. Chem.*, 2014, **86**, 592–599.
36 DiffAtOnce® is a registered program developed by I. Fernández and F. M. Arrabal-Campos in the University of Almería, 2013, and available at **https://www.diffatonce.com/**.
37 P. V. Giampouras, K. E. Themelis, A. A. Rontogiannis and K. D. Koutroumbas, *IEEE Trans. Geosci. Remote Sens.*, 2016, **54**, 4775–4789.
38 B. Yuan, Y. Ding, G. M. Kamal, L. Shao, Z. Zhou, B. Jiang, P. Sun, X. Zhang and M. Liu, *J. Magn. Reson.*, 2017, **278**, 1–7.
39 R. J. Woods group, web address: **https://glycam.org/**, 2005–2024.
40 C. I. Bayly, P. Cieplak, W. D. Cornell and P. A. Kollman, *J. Phys. Chem.*, 1993, **97**, 10269–10280.
41 T. Darden, Y. Darrin and P. Lee, *J. Chem. Phys.*, 1993, **98**, 10089–10092.